THREE DIMENSIONAL WATER FLOW IN NOZZLES

Johannes V. Soulis[1], Modestos A. Loukas[2]

[1]Fluid Mechanics/Hydraulics Division, Department of Civil Engineering,
Democrition University of Thrace,
Xanthi, GR-67100, Greece
e-mail: soulis@civil.duth.gr

[2]Fluid Mechanics/Hydraulics Division, Department of Civil Engineering,
Democrition University of Thrace,
Xanthi, GR-67100, Greece
e-mail: modloukas@yahoo.com

Keywords: Euler Equations, Finite-volume Method, Turbomachinery Flows.

Abstract: *A time-marching finite-volume numerical procedure is presented for three-dimensional incompressible turbomachinery flows. The code (D3flow) is applied to the conservative form of the Euler equations written in general curvilinear co-ordinates. A simple but computational efficient grid is constructed. Numerical solution results for 3D nozzle, shown in Figures 1, 3 and 4, are presented and compared with the Fluent (ANSYS 14.5 program released in 2012), Figures 5-12. Predicted results using either method yield satisfactory comparison. The proposed numerical method is an accurate and reliable technique for solving inviscid, incompressible flow equations in 3D turbomachinery geometries.*

1 INTRODUCTION

Turbomachinery development of either pumps or turbines has been largely conditioned by the improvements achieved in component efficiencies. Design and performance estimation of pumps and turbines has been based and will continue to be so, almost completely, on the understanding of fluid flow behavior. However, flow passages through turbomachines are geometrically very complex and the interaction between rotors and stationary parts constitutes a major challenge.

Computational fluid dynamics methodology applied to turbomachinery flows has been achieved a considerable progress in the past several years. Although efficient algorithms are now available to integrate the Navier-Stokes equations, this appears to be still a formidable task for purposes of practical applications. In the complex turbomachine environment the prediction accuracy of such flow calculations is limited by the limitations of turbulence modelling. Mixing length eddy viscosity models are by far the most commonly used method[1]. The solution of inviscid flows (Euler equations) through turbomachinery passages is a good first approximation for analysis. It is of practical interest for the design of turbomachinery components. Inviscid flow equations are numerically treated in two distinct categories, namely Euler solvers and potential flow (irrotational) solvers. Potential methods do not appear to have been widely used for design purposes. Nowadays, 3D Euler solvers are well developed and are available for routine turbomachinery calculations. Several of these dealing with internal and external flows are described by Hirsch[2]. Euler solvers for 3D turbomachinery flows have been reported as early as 1974 by Denton[3], who developed an explicit time-marching method. His widely accepted method employs an opposed difference scheme in order to solve the Euler equations. The scheme uses upwind differencing for fluxes of mass and momenta, but downwind differences for pressures in the streamwise direction. In addition, correction factors for each of the physical quantities are applied in the streamwise direction. The method is of the finite-volume type. Numerical solution techniques were presented by Shieh and Delanay[4]. The hop-scotch scheme was applied to the conservative form of the Euler equations written in general curvilinear co-ordinates using an O-type grid system. Weber et al[5] presented a 3D Euler analysis on a C-type grid using the well-known Beam-Warming implicit algorithm. Results for a cascade and rotor flows were presented. Arts[6] presented an inviscid flow solution for axial turbine stage. Holmes and Tong[7] described a 3D Euler solver for turbomachinery blade rows. The algorithm was based on the explicit, four-step, Runge-Kutta finite-volume method advocated by Jameson.

The objective of this paper is to outline an accurate and efficient numerical procedure for simulating the time-averaged, 3D, inviscid water flow field within a typical turbomachinery nozzle. The main scope was to

calculate flows through all types of turbomachines (axial, mixed, radial) no matter how complex their geometry may be. The proposed scheme has several advantages:

a. The grid used is the simplest possible formation for numerical calculations.
b. The conservative form of the equations is written in general curvilinear co-ordinates, thus enabling complex geometry to be efficiently analyzed.
c. Calculated water mass flows into and out of the nozzle are matched.
d. Boundary conditions are easily and accurately satisfied in a straight forward manner.
e. The time integration numerical procedure is a straightforward method requiring minimal algorithm coding.
f. Artificial viscosity is provided via a simple pressure correction formula.

For the time being applications are restricted to water flow through nozzles with 3D complex geometry. The computer code development was performed at the Computation Laboratory of the Fluid Mechanics/Hydraulics Division, Civil Engineering Department, Democrition University of Thrace.

2 GOVERNING FLOW EQUATIONS

The basic equations governing the flow inside of any turbomachine are derived from the principles of conservation of mass, momentum and energy. It is convenient to write the 3D Euler equations in a cylindrical polar co-ordinate system (z, θ, r). Since the algorithm was developed for compressible fluid analysis, it is convenient to write down the equations in compressible flow (taking into account the rotation) and to treat the incompressible flow as part of it for water flow analysis. These equations are expressed in conservation form as

$$-\frac{\partial(r\rho)}{\partial t}=\frac{\partial(r\rho u)}{\partial z}+\frac{\partial[\rho(\upsilon-r\Omega)]}{\partial\theta}+\frac{\partial(r\rho w)}{\partial r}, \tag{1}$$

$$-\frac{\partial(r\rho u)}{\partial t}=\frac{\partial[r(\rho u^2+p)]}{\partial z}+\frac{\partial[\rho(\upsilon-r\Omega)u]}{\partial\theta}+\frac{\partial(r\rho uw)}{\partial r}, \tag{2}$$

$$-\frac{\partial(r\rho\upsilon)}{\partial t}=\frac{\partial(r\rho u\upsilon)}{\partial z}+\frac{\partial[\rho(\upsilon-r\Omega)u+p]}{\partial\theta}+\frac{\partial(r\rho\upsilon w)}{\partial r}+\rho\upsilon w, \tag{3}$$

$$-\frac{\partial(r\rho w)}{\partial t}=\frac{\partial(r\rho uw)}{\partial z}+\frac{\partial[\rho(\upsilon-r\Omega)w]}{\partial\theta}+\frac{\partial[r(\rho w^2+p)]}{\partial r}-(p+\rho\upsilon^2), \tag{4}$$

$$-\frac{\partial(r\rho e)}{\partial t}=\frac{\partial[r(\rho e+p)u]}{\partial z}+\frac{\partial[(\rho e+p)\upsilon-e\rho r\Omega)]}{\partial\theta}+\frac{\partial[r(\rho e+p)w]}{\partial r}, \tag{5}$$

z, θ and r are the axial, tangential and radial directions respectively, t is the time, ρ is the density, u, υ and w are the absolute velocity components along the z-, θ- and r- directions respectively, p is the pressure of the fluid, Ω is the rotational speed of the impeller and e is the total internal energy given by the equation below,

$$e=\frac{p}{\rho(\gamma-1)}+\frac{1}{2}(u^2+\upsilon^2+w^2), \tag{6}$$

γ is the ratio of the specific heats. The unknowns of the problem are the six physical quantities u, υ, w, ρ, p and e. The problem must be closed with a complete specification of the boundary conditions.

Upstream conditions

The stagnation at the inlet flow is assumed to be constant throughout the streamwise direction.

Downstream conditions

The static pressure is set on the hub surface and the radial pressure distribution is determined by the simple radial equilibrium equation,

$$\frac{\partial p}{\partial r} = \frac{\rho v^2}{r} \tag{7}$$

3 MESH GENERATION

A complex grid system was developed and implemented on the main numerical method to allow flows inside complex geometry to be calculated. An example of a complex geometry which was used for analysis is shown in Figure 1a. Hub and casing radial co-ordinates along the machine axis are provided as an input to the computer code. Input cross-sections are interpolated to calculate the axial, suction surface and blade thickness. Meridional grid points are uniformly spaced in the r-direction. Axial points need not be equally spaced. Figure 1b shows the 3D grid used for nozzle analysis (Fluent). Use of pitchwise lines greatly simplifies the application of the periodic boundary properties between the bounding quasi-streamlines of the passage. However, the numerical scheme can be used with any grid formation, which need not be uniformly spaced in any co-ordinate direction. The grid is not restricted to the one described. Any mesh generation technique can be adopted. Edges require special numerical treatment. The problem can be overcome by fitting more grid points where appropriate. The D3flow program utilizes 2800 nodes while the Fluent 53361 nodes.

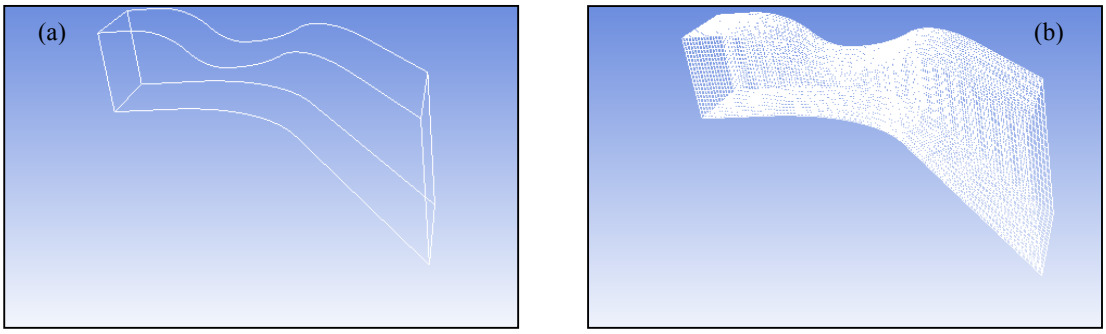

Figure 1. (a) Geometry of the 3D nozzle, (b) mesh used for analysis (Fluent)

4 TRANSFORMATION EQUATIONS

The discrete approximation to the governing flow equation has been developed by dividing the physical domain into cuboid cells which can be defined arbitrarily to produce surface-fitted grids, the structure of which follows the turbomachinery internal configuration. Once this has been achieved, a transformation is introduced through which cuboids of the physical domain are mapped into computational domain cubes, Figure 2, Soulis[7].

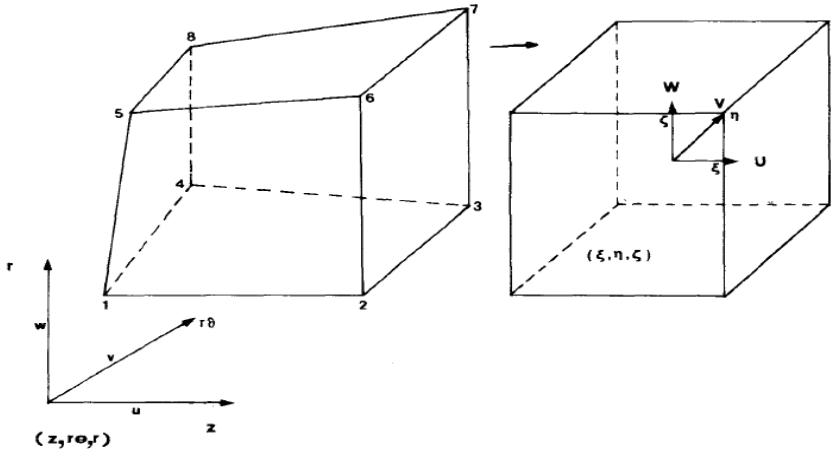

Figure 2. Distorted cubes of the physical domain are mapped into cubes of the computational domain

The transformation from global z, θ, r to local ξ, η, ζ co-ordinates can be expressed as,

$$z = \sum_{i=1}^{8} N_i z_i,\ \theta = \sum_{i=1}^{8} N_i \theta_i,\ \ r = \sum_{i=1}^{8} N_i r_i, \tag{8}$$

N_i are the first-order, linear shape functions associated with the cuboid nodes, Soulis et al.[8] . The use of first-order shape functions has been determined by the necessity to restrict the complexity of the numerical code, which is inherent to almost all 3D computational methods. Thus, in order to numerically solve the system of governing flow equations (1) – (6) on a body-fitted grid system, the equations are transformed to an arbitrary curvilinear system:

$$-\frac{\partial(rJ^{-1}\rho)}{\partial t} = \frac{\partial(rJ^{-1}\rho U)}{\partial \xi} + \frac{\partial(rJ^{-1}\rho V)}{\partial \eta} + \frac{\partial(rJ^{-1}\rho W)}{\partial \zeta}, \tag{9}$$

$$-\frac{\partial(rJ^{-1}\rho u)}{\partial t} = \frac{\partial[rJ^{-1}(\rho uU + \xi_z p)]}{\partial \xi} + \frac{\partial[rJ^{-1}(\rho uV + \eta_z p)]}{\partial \eta} + \frac{\partial[rJ^{-1}(\rho uW + \zeta_z p)]}{\partial \zeta}, \tag{10}$$

$$-\frac{\partial(rJ^{-1}\rho \upsilon)}{\partial t} = \frac{\partial[rJ^{-1}(\rho \upsilon U + \xi_\theta p / r)]}{\partial \xi} + \frac{\partial[rJ^{-1}(\rho \upsilon V + \eta_\theta p / r)]}{\partial \eta} + \frac{\partial[rJ^{-1}(\rho \upsilon W + \zeta_\theta p / r)]}{\partial \zeta} + J^{-1}\rho \upsilon W, \tag{11}$$

$$-\frac{\partial(rJ^{-1}\rho w)}{\partial t} = \frac{\partial[rJ^{-1}(\rho wU + \xi_r p)]}{\partial \xi} + \frac{\partial[rJ^{-1}(\rho wV + \eta_r p)]}{\partial \eta} + \frac{\partial[rJ^{-1}(\rho wW + \zeta_r p)]}{\partial \zeta} - J^{-1}(\rho \upsilon^2 + p), \tag{12}$$

$$-\frac{\partial(rJ^{-1}\rho e)}{\partial t} = \frac{\partial\{rJ^{-1}[(\rho e + p)U + \xi_\theta p(r\Omega)/r)]\}}{\partial \xi} + \frac{\partial\{rJ^{-1}[(\rho e + p)V + n_\theta p(r\Omega)/r)]\}}{\partial \eta} + \frac{\partial\{rJ^{-1}[(\rho e + p)W + \zeta_\theta p(r\Omega)/r)]\}}{\partial \zeta}, \tag{13}$$

U, V and W are the contravariant velocity components in the ξ-, η- and ζ- directions, respectively. The inverse Jacobian J^{-1} of the transformation from the physical to the local co-ordinate system is defined, Soulis[9], as,

$$J^{-1} = \begin{bmatrix} z_\xi & z_\eta & z_\zeta \\ \theta_\xi & \theta_\eta & \theta_\zeta \\ r_\xi & r_\eta & r_\zeta \end{bmatrix}. \tag{14}$$

The metrics ξ_z, η_z and ζ_z, of eq. (10) are,

$$\xi_z = (\theta_\eta r_\zeta - r_\eta \theta_\zeta)/J^{-1},\ \eta_z = (r_\xi \theta_\zeta - \theta_\xi r_\zeta)/J^{-1},\ \zeta_z = (\theta_\xi r_\eta - \theta_\eta r\xi)/J^{-1}. \tag{15}$$

Similarly the metrics ξ_θ, η_θ and ζ_θ, of eq. (11) are,

$$\xi_\theta = (z_\zeta r_\eta - z_\eta r_\zeta)/J^{-1},\ \eta_\theta = (z_\xi r_\zeta - z_\zeta r_\xi)/J^{-1},\ \zeta_\theta = (z_\eta r_\xi - z_\xi r_\eta)/J^{-1}, \tag{16}$$

the metrics ξ_r, η_r and ζ_r, of eq. (12) are,

$$\xi_r = (z_\eta \theta_\zeta - z_\zeta \theta_\eta)/J^{-1},\ \eta_r = (z_\zeta \theta_\xi - z_\xi \theta_\zeta)/J^{-1},\ \zeta_r = (z_\xi \theta_\eta - z_\eta \theta_\xi)/J^{-1}. \tag{17}$$

The contravariant velocities are related to the physical velocities by the equations,

$$U = \xi_z u + (\frac{\xi_\theta}{r})(\upsilon - r\Omega) + \xi_r w, \tag{18}$$

$$V = \eta_z u + (\frac{\eta_\theta}{r})(\upsilon - r\Omega) + \eta_r w, \tag{19}$$

$$W = \zeta_z u + (\frac{\zeta_\theta}{r})(\upsilon - r\Omega) + \zeta_r w. \tag{20}$$

In all the above equations the subscripts *z, θ* and *r* refer to partial derivatives. Then, a numerical algorithm is being used to solve the governing flow eqs. (9)-(13), Soulis[10]. Convergence is achieved when all physical quantities (plus the mass balance) reaches a 10^{-7} accuracy.
In order to achieve the desired convergence, the D3flow program uses 5 factors:

a. *FT* (=1.0) is an iteration step factor determining the iteration step.
b. *SF* (=0.012) is a smoothing factor acting on changes of the velocities and pressure.
c. *OMIN* (=0.15) is a relaxation factor acting on pressure changes updating flow conditions at inlet.
d. *FACT1* (=0.1) is a multiplication factor applied over continuity equation updating pressure.
e. *FACT2* (=0.025) is a multiplication factor applied over axial, tangential and radial momentum equations updating the axial, tangential and radial velocities.

5 GEOMETRY

The geometry of the 3D nozzle is shown in figures 3 (side view) and 4 (top view), Loukas[11]. To construct the nozzle geometry the radius *r* in equation (7) attains high value so as the pressure variation across the radius at the outlet to be negligible.

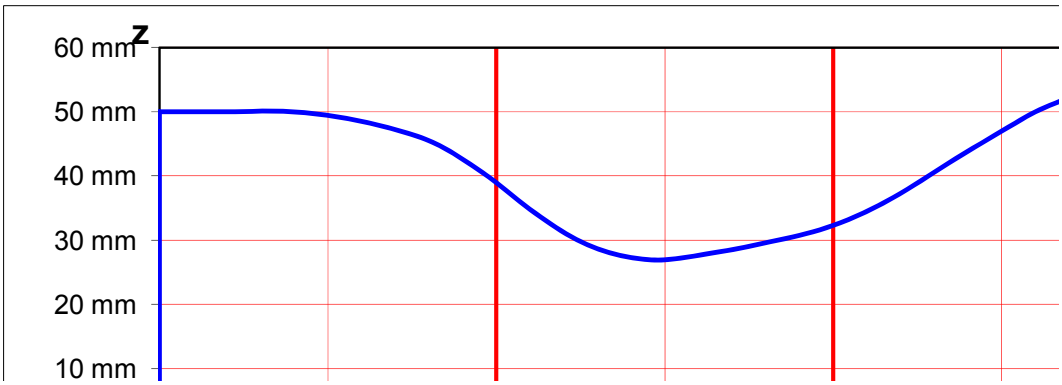

Figure 3. Geometry of the side view for the 3D nozzle

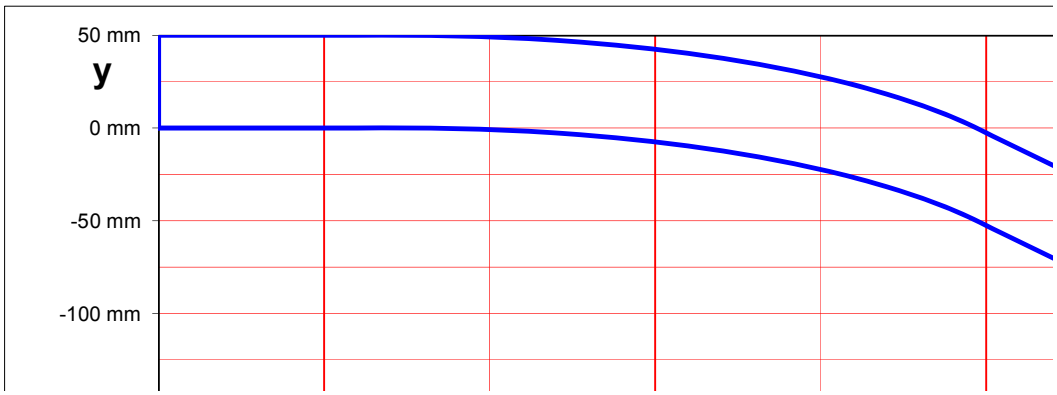

Figure 4. Geometry of the top view for the 3D nozzle

6 BOUNDARY – INITIAL CONDITIONS

To achieve the most favourable comparisons between applied methods, the outlet D3flow boundary conditions are accordingly adjusted. The boundary conditions for the 3D nozzle problem using D3flow and Fluent technique are shown in table 1.

	Fluent	D3flow
Static pressure at inlet	140000.0 Pa	140000.0 Pa
Static pressure at outlet	101000.0 Pa	101000.0 Pa
Total pressure at inlet	144000.0 Pa	144000.0 Pa
Boundaries	Solid (perpendicular velocities are set zero)	Solid (perpendicular velocities are set zero)
Fluid density (water) ρ	1000.0 kg/m^3	1000.0 kg/m^3
Gravity acceleration g	9.81 m/s^2	9.81 m/s^2
Dynamic (shear) viscosity μ	0.0 kg/m-s	0.0 kg/m-s

Table 1 : Boundary conditions using D3flow and Fluent numerical techniques

NOTES:

a. Gravity acceleration g has negligible effects upon the solution in either program.
b. The flow is assumed to be inviscid (μ=0.0 kg/m-s).
c. The rotational speed Ω is set equal to zero.

7 COMPUTATIONAL RESULTS

The current research work presents the results of solving the 3D nozzle problem using Fluent and D3flow. The computational static pressure distribution comparison between the methods D3flow and Fluent are shown in figures 5,6,7 and 8 for bottom-right side, bottom-left side, upper-right side and upper-left side, respectively.

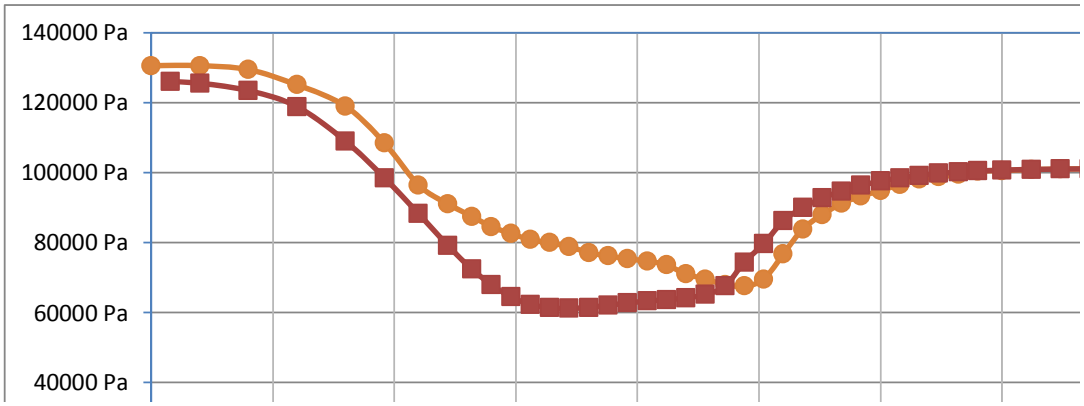

Figure 5. Static pressure (Pa) distribution comparing D3flow–Fluent results for bottom–right side

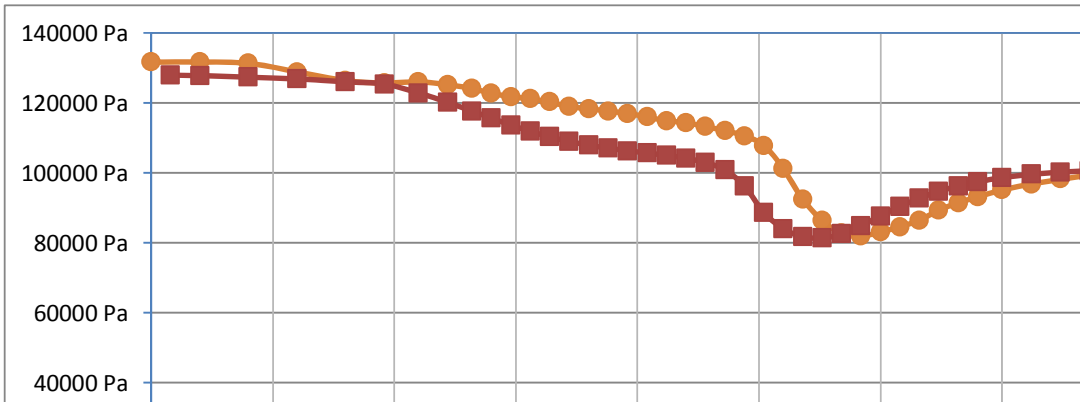

Figure 6. Static pressure (Pa) distribution comparing D3flow–Fluent results for bottom–left side

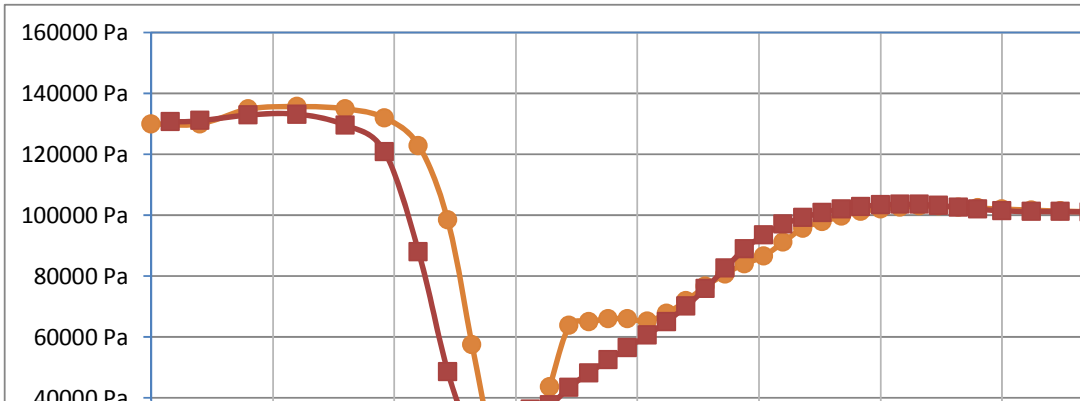

Figure 7. Static pressure (Pa) distribution comparing D3flow–Fluent results for upper–right side

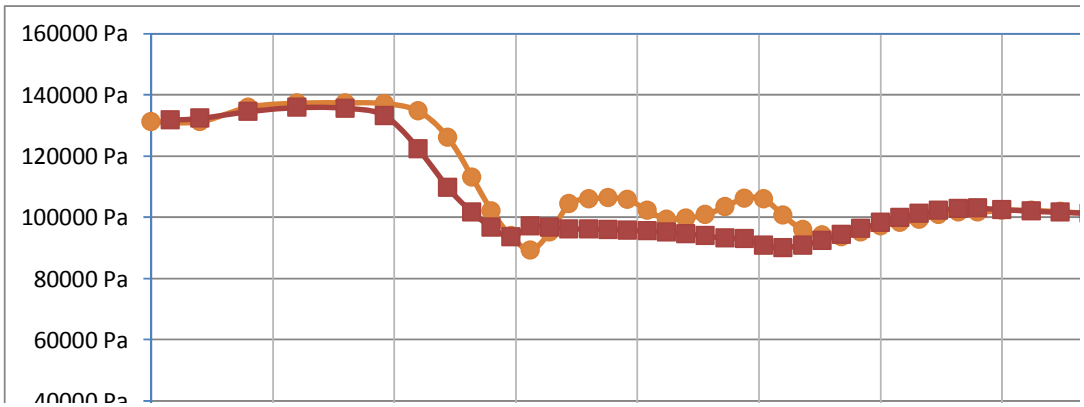

Figure 8. Static pressure (Pa) distribution comparing D3flow–Fluent results for upper–left side

The computational total velocity distribution comparison between the methods D3flow and Fluent are shown in figures 9, 10, 11 and 12 for bottom right-side, bottom-left side, upper-right side and upper-left side, respectively.

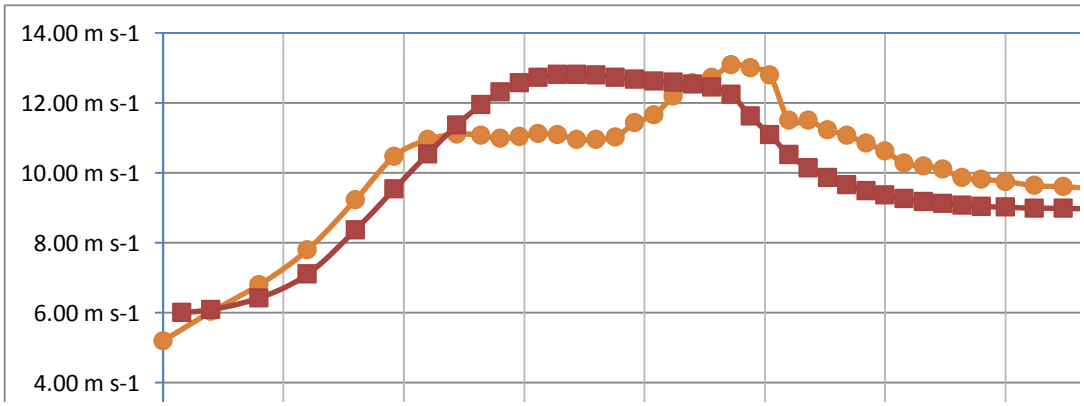

Figure 9. Velocity magnitude (m/s) distribution comparing D3flow–Fluent results for bottom–right side

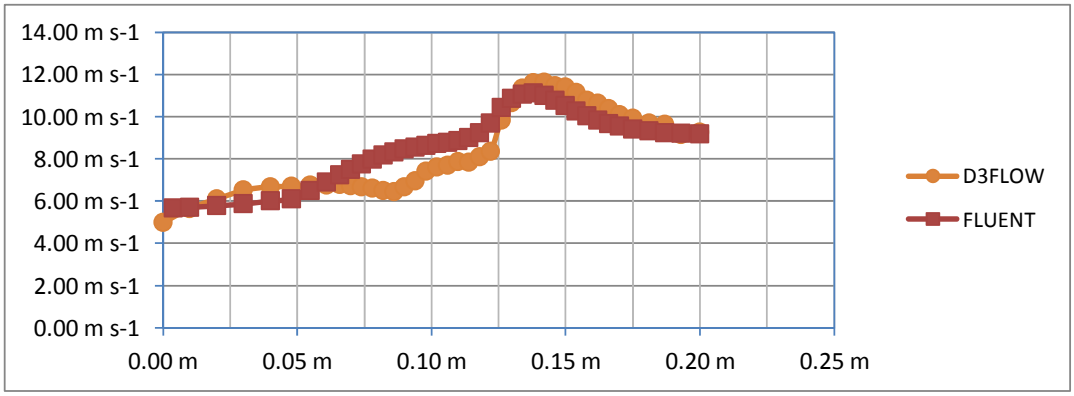

Figure 10. Velocity magnitude (m/s) distribution comparing D3flow–Fluent results for bottom–left side

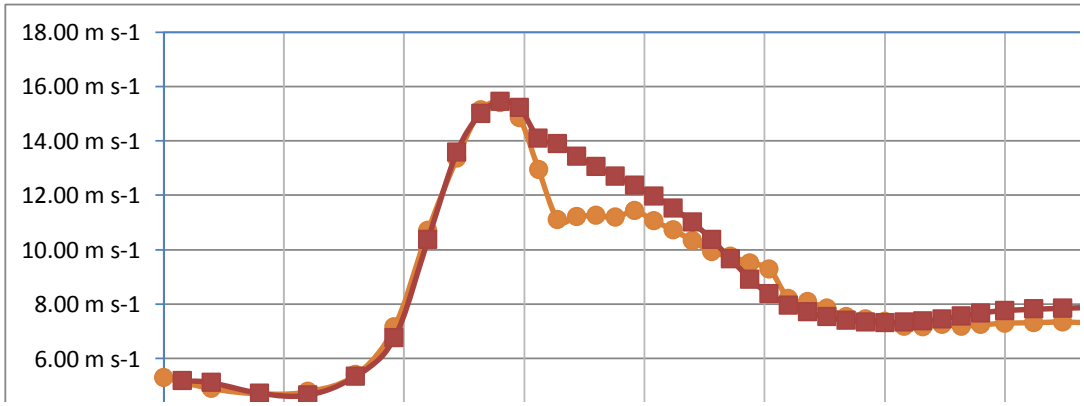

Figure 11. Velocity magnitude (m/s) distribution comparing D3flow–Fluent results for upper – right side

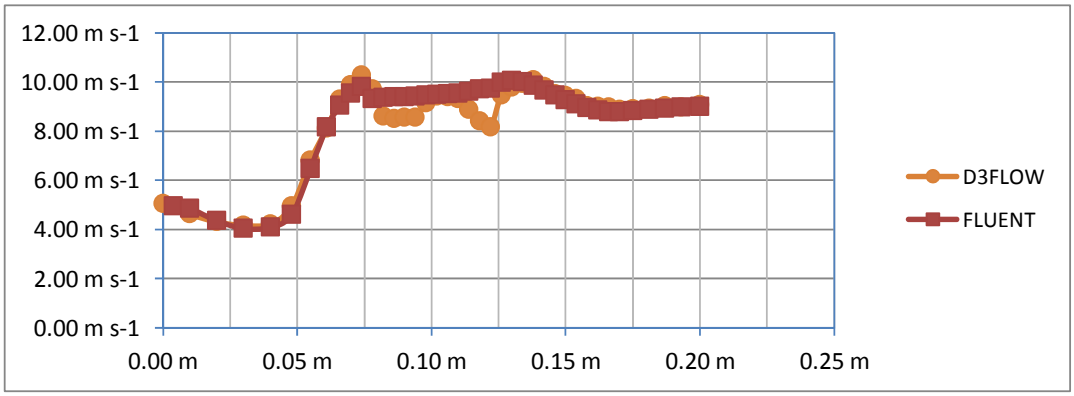

Figure 12. Velocity magnitude (m/s) distribution comparing D3flow–Fluent results for upper–left side

8 DISCUSSION

From the geometry of the 3D nozzle, figure 3, it is clear that the z axis attains the height of 50.0 mm at inlet (x=0.0 mm) and keeps it up to x=19.0 mm, then the geometry convergence starts and ends at x=75.0 mm, where "throat" is formed. Thereafter, divergence starts ending at x=150.0 mm. From the distance of x=150.0 mm up to the exit of the nozzle the height attains 60.0 mm.

a. Reduction in the static pressure occurs from inlet up to the distance of x=120.0 mm ("throat") at the bottom-right side of the nozzle. Then, the static pressure attains small changes for a short axial distance. Thereafter, an increase in the static pressure occurs up to the outlet of the nozzle, figure 5.
b. Reduction in the static pressure occurs from the inlet up to the distance of x=130.0 mm and then starts increasing up to the end of the nozzle at the bottom-left side, figure 6. Contours of static pressure (Pa) at the bottom side using Fluent are shown in figure 13.
c. Drop of static pressure occurs reaching its lowest value at x=75.0 mm at the upper-right side, figure 7. Thereafter, the static pressure is recovered.
d. Drop of static pressure also occurs reaching its lowest value at x=75.0 mm at the upper-left side, figure 8. However, the low static value for this side of the nozzle is considerable milder to the one appearing in upper-right side, figure 7. There is pressure recovering after x=75.0 mm. The pressure keeps this value which was attained at the "throat" of the nozzle. Contours of static pressure at the upper side using Fluent are shown in figure 14. The low static pressure is clearly depicted by blue colour.
e. The velocity distribution is almost "inversely proportional" to the static pressure[11] changes, figures 5-12.

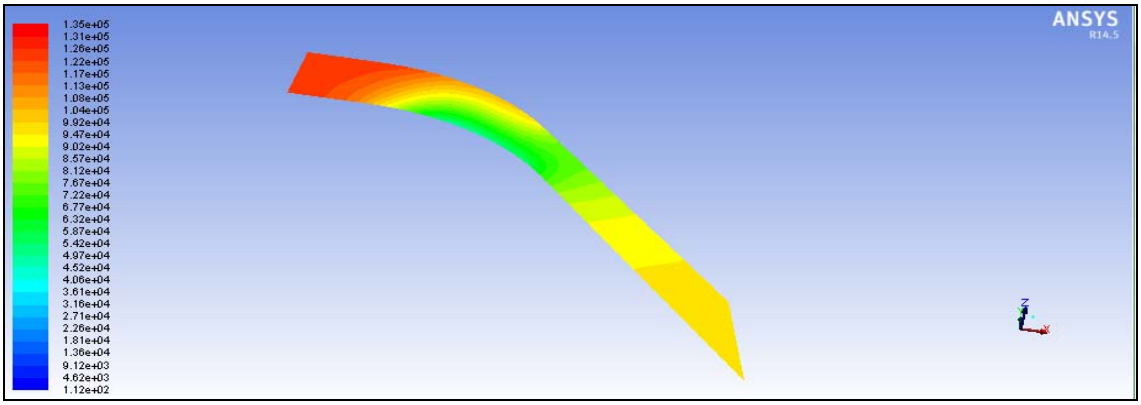

Figure 13. Contours of static pressure (Pa) at the bottom side using Fluent

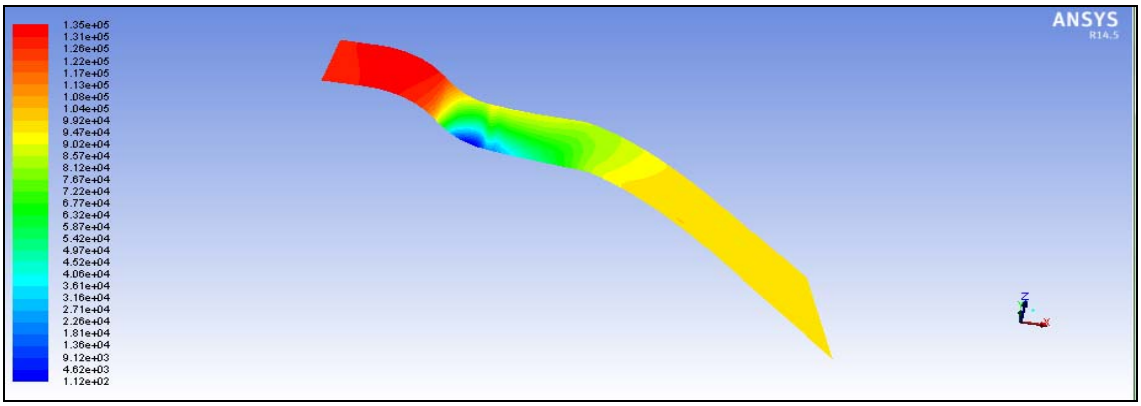

Figure 14. Contours of static pressure (Pa) at the upper side in Fluent

9 CONCLUSIONS

The computational results using the two programs are very close to each other so it can be assumed that the predicted results of the program D3flow are close to reality. Only experiential results can show the accuracy of the predictions always under the assumption made about the flow. The code is based on a simple body-conforming grid system. It utilizes a simple time integration technique. The program has been tested on a nozzle exhibiting a 3D flow structure. Comparisons with Fluent predictions demonstrate the accuracy and computational efficiency of the method. Main features of the flow are reasonably well predicted, even using comparatively coarse grids. However, much finer grids would be needed to resolve details of the complex 3D nozzle geometry. Whenever convergence problems have occurred, they have always been traced to bad grids and have vanished when the grid was refined.

REFERENCES

[1] Denton, J. D. (1990), "The calculation of three-dimensional viscous flow through multistage turbomachines", *ASME Paper*, 90-GT-19.

[2] Hirsch, C. (1990), "*Numerical Computation of Internal and External Flows*", Vol. 2, Wiley, Chichester, Chap. 16, pp. 132-583.

[3] Denton, J. D. (1974), "A time-marching method for two-dimensional and three-dimensional blade to blade flows", *ARC R&D 3775.*

[4] Shieh, C. F., Delaney, R. A. (1986), "An accurate and efficient Euler solver for three-dimensional turbomachinery flows", *ASME Paper,* 86-GT-200.

[5] Weber, K. F. , Thoe D. W., Delaney, R. A. (1990), "Analysis of three-dimensional turbomachinery flows on C-type grids using an implicit Euler solver", *Journal Turbomachinery,* 112, pp. 362-369.

[6] Arts, T. (1985), "Calculation of the three-dimensional steady inviscid flow in a transonic axial turbine stage", *ASME Paper,* 84- GT-76.

[7] Soulis, J. V. (1983), "Finite-volume method for three-dimensional transonic potential flow through turbomachinery blade rows", *Int. J. Heat Fluid Flow*, 4.

[8] Soulis, J. V. , Bellos, K. V. (1988), "Conservation form of fluid dynamics equations in curvilinear coordinate systems, Part I, Mathematical analysis", *Tech. Chron. B*, 8, (4), pp. 69-97.

[9] Soulis, J. V. (1986), *Computational Fluid Mechanic*s, Democrition University of Thrace, Civil Engineering Department, Thessaloniki, Aivazis–Zouboulis.

[10] Soulis, J. V. (1995), "An Euler solver for three-dimensional turbomachinery flows", *International Journal for Numerical Methods in Fluids,* vol.20, pp. 1-30.

[11] Loukas, M. A., (2015), *3D flow in turbomachinery nozzles*, Democrition University of Thrace, Civil Engineering Department, Xanthi.